Inorganic Chemistry
Article

Inorg. Chem. **2010**, *49*, 8411–8420 **8411**
DOI: 10.1021/ic100919a

Continuous Shape- and Spectroscopy-Tuning of Hematite Nanocrystals

Liqiao Chen, Xianfeng Yang, Jian Chen, Jia Liu, Hao Wu, Hongquan Zhan, Chaolun Liang, and Mingmei Wu*

State Key Laboratory of Optoelectronic Materials and Technologies/MOE Key Laboratory of Bioinorganic and Synthetic Chemistry, School of Chemistry and Chemical Engineering and Instrumental Analysis and Research Center, Sun Yat-Sen University, Guangzhou 510275, P. R. China

Received May 7, 2010

Uniform hexagonal hematite (α-Fe_2O_3) nanoplates have been synthesized by a facile alcohol-thermal reaction, and a new nanostructure of α-Fe_2O_3 has been proposed. Each nanoplate is enclosed by (0001) basal planes and $\{10\bar{1}2\}$ side surfaces. The phase, size, shape, and growth orientation of these nanocrystals were characterized by powder X-ray diffraction and electron microscopy. The thickness and diameter of these nanocrystals could be finely tuned by the selective use of alcohol solvent with increasing carbon atom number in the linear alkyl chain. A variety of nanocrystals with systemically changeable shapes from nanoplates to nanograins have been obtained. Specific adsorption of alcohol molecules on polar (0001) facets is proposed to be the main issue to modify the growth behavior of hematite nanocrystals. The presence of distilled water and the addition of sodium acetate have also been investigated. Either of them has a great influence on the growth of hematite nanocrystals, and shape-controlled growth can be rationally achieved. In addition, the post-aging of as-grown hematite nanocrystals in alcohol and distilled water has also been described. Both vibration spectroscopy (i.e., FTIR and Raman) and electronic spectra (diffused reflectance spectra) of these nanocrystals with a continuing shape change show a highly shape-dependent nature.

I. Introduction

It has been well established that the properties and performances of nanostructured materials are dependent not only on their chemical composition and inherent crystallographic structure, but also on morphology, crystal size, and growth orientation. Nanosized crystals can offer us a feasible opportunity for systematically studying and tuning their size- and shape-dependent properties. Many efforts have been devoted to controlled growth, growth mechanism, and nanostructure-related properties of functional nanocrystals.[1] Fe_2O_3 is one of the simplest oxides on first impression, which usually exists in nature in two polymorphs: cubic γ-Fe_2O_3 and rhombohedral α-Fe_2O_3.[2] Because of its instinctive environmentally friendly, nontoxic, corrosion-resistant features, thermal stability, and profound performances, hematite (i.e., α-Fe_2O_3) as a well-known magnetic semiconductor with a band gap of around 2.1 eV has many potential applications in optical, magnetic, electrochemical, and (photo)-catalytic fields compared to most of the other oxides.[3−12] It has been

*To whom correspondence should be addressed. E-mail: ceswmm@mail.sysu.edu.cn.

(1) (a) Kwon, S. G.; Hyeon, T. *Acc. Chem. Res.* **2008**, *41*, 1696–1709. (b) Jun, Y.-W.; Choi, J.-S.; Cheon, J. *Angew. Chem., Int. Ed.* **2006**, *45*, 3414–3439. (c) Xia, Y. N.; Xiong, Y. J.; Lim, B.; Skrabalak, S. E. *Angew. Chem., Int. Ed.* **2009**, *48*, 60–103. (d) Burda, C.; Chen, X. B.; Narayanan, R.; El-Sayed, M. A. *Chem. Rev.* **2005**, *105*, 1025–1102. (e) Goesmann, H.; Feldmann, C. *Angew. Chem., Int. Ed.* **2010**, *49*, 1362–1395. (f) Pinna, N.; Niederberger, M. *Angew. Chem., Int. Ed.* **2008**, *47*, 5292–5304. (g) Yin, Y.; Alivisatos, A. P. *Nature* **2005**, *437*, 664–670. (h) Lisiecki, I. *J. Phys. Chem. B* **2005**, *109*, 12231–12244.

(2) (a) Cornel, R. M.; Schwertmann, U. *The Iron Oxides. Structure, Properties, Reactions, Occurrences and Uses*; Wiley-VCH: Weinheim, Germany, 2003. (b) Zboril, R.; Mashlan, M.; Petridis, D. *Chem. Mater.* **2002**, *14*, 969–982. (c) Sakurai, S.; Namai, A.; Hashimoto, K.; Ohkoshi, S.-I. *J. Am. Chem. Soc.* **2009**, *131*, 18299–18303.

(3) (a) Kay, A.; Cesar, I.; Gratzel, M. *J. Am. Chem. Soc.* **2006**, *128*, 15714–15721. (b) Zhong, D. K.; Sun, J. W.; Inumaru, H.; Gamelin, D. R. *J. Am. Chem. Soc.* **2009**, *131*, 6086–6087. (c) Formal, F. L.; Gratzel, M.; Sivula, K. *Adv. Funct. Mater.* **2010**, *20*, 1099–1107. (d) Hahn, N. T.; Ye, H. C.; Flaherty, D. W.; Bard, A. J.; Mullins, C. B. *ACS Nano* **2010**, *4*, 1977–1986.

(4) (a) Liu, Q.; Cui, Z. M.; Ma, Z.; Bian, S. W.; Song, W. G.; Wan, L. J. *Nanotechnology* **2007**, *18*, 1–5. (b) Xu, H.; Wang, X. B.; Zhang, L. Z. *Powder Technol.* **2008**, *185*, 176–180. (c) Shaikh, N. S.; Enthaler, S.; Junge, K.; Beller, M. *Angew. Chem., Int. Ed.* **2008**, *47*, 2497–2501. (d) Formal, F. L.; Grätzel, M.; Sivula, K. *Adv. Funct. Mater.* **2010**, *20*, 1099–1107.

(5) Zheng, Y. H.; Cheng, Y.; Wang, Y. S.; Bao, F.; Zhou, L. H.; Wei, X. F.; Zhang, Y. Y.; Zheng, Q. *J. Phys. Chem. B* **2006**, *110*, 3093–3097.

(6) (a) Chen, J.; Xu, L. N.; Li, W. Y.; Gou, X. L. *Adv. Mater.* **2005**, *17*, 582–586. (b) Wu, C. Z.; Yin, P.; Zhu, X.; Ouyang, C. Z.; Xie, Y. *J. Phys. Chem. B* **2006**, *110*, 17806–17812.

(7) Hu, X. L.; Yu, J. C.; Gong, J. M.; Li, Q.; Li, G. S. *Adv. Mater.* **2007**, *19*, 2324–2329.

(8) (a) Reddy, M. V.; Yu, T.; Sow, C. H.; Shen, Z. X.; Lim, C. T.; Rao, G. V. S.; Chowdari, B. V. R. *Adv. Funct. Mater.* **2007**, *17*, 2792–2799. (b) Zhou, J. S.; Song, H. H.; Chen, X. H.; Zhi, L. J.; Yang, S. Y.; Huo, J. P.; Yang, W. T. *Chem. Mater.* **2009**, *21*, 2935–2940.

(9) Zheng, Z.; Liao, L.; Yan, B.; Zhang, J. X.; Gong, H.; Shen, Z. X.; Yu, T. *Nanoscale Res. Lett.* **2009**, *4*, 1115–1119.

(10) (a) Cao, S. W.; Zhu, Y. J. *J. Phys. Chem. C* **2008**, *112*, 6253–6257. (b) Zeng, S. Y.; Tang, K. B.; Li, T. W.; Liang, Z. H.; Wang, D.; Wang, Y. K.; Zhou, W. W. *J. Phys. Chem. C* **2007**, *111*, 10217–10225. (c) Zhong, L. S.; Hu, J. S.; Liang, H. P.; Cao, A. M.; Song, W. G.; Wan, L. *J. Adv. Mater.* **2006**, *18*, 2426–2431. (d) Cai, W. Q.; Yu, J. G.; Cheng, B.; Su, B. L.; Jaroniec, M. *J. Phys. Chem. C* **2009**, *113*, 14739–14746.

Published on Web 08/18/2010

used in photo anode,[3] catalyst,[4,5] gas sensors,[6,7] Li-ion batteries,[6,8] field emission,[9] environmental protection,[10] magnetic field,[11] pigments (dyes),[12] and so on in the literature.

In addition to their highly size-dependent performance,[13,14] α-Fe_2O_3 nanocrystals exhibit abundant shape- and orientation-dependent physical and even chemical properties.[5,12,15] Thus, the rational growth of uniform α-Fe_2O_3 nanocrystals is quite important in understanding these nanostructural parameter-dependent properties. In the past few years, great progress has been made in the chemical growth of uniform α-Fe_2O_3 nanocrystals with a variety of specific shapes and morphologies.[16−24] First, some organic surfactants were adopted to modify growth behavior to obtain some specific nanostructured materials. For example, quasi-cubic α-Fe_2O_3 nanocrystals were obtained with the assistance of PVP as a surfactant.[5] Under the assistance of CTAB surfactant, α-Fe_2O_3 nanorods with polyhedral configuration were grown by Jia and his coauthors.[17] These nanorods were bounded by (104) facets as the top surfaces and (012) planes as side ones. A second way to design the growth approach is the use of some anions, either organic or inorganic. It was found that the presence of phosphate anions in the growth medium could lead to systematic shape modification of one-dimensional nanostructures. Typically, continuing shape-controlled growth of α-Fe_2O_3 nanocrystals with a morphological change from uniform nanocubes to nanospindles has been achieved by Yu and his coauthors with the use of variable phosphate contents in the reaction media.[18] These nanocrystals demonstrated tunable shape-related infrared spectra, which was similar as those size-related ones.[14] Initial molar ratio of Fe^{3+} to PO_4^{3-} also plays a crucial role in the final tubular and like a circle α-Fe_2O_3 nanocrystals as reported by Yan et al.[19] Sulfate ions were also found to be able to modify the shape of hexagonal nanocrystals under different pH values. This is because of their selectively adsorbing to some defined crystal faces at different conditions.[20] It was proposed that nitrilotriacetic acid (NTA) could serve as a chelating agent to form polymeric chains to confine the growth of some specific lattice planes, and consequently α-Fe_2O_3 nanowires were obtained.[21] On the basis of another strategy by modifying nucleation rate and aging time, size- and shape-controlled growth was achieved through varying the starting Fe^{3+} concentrations in the reaction system.[22] A typical example is the shape transformation of α-Fe_2O_3 nanocrystals from irregular spheres, quasi-rhombs, and truncated cubes, to finally pseudocubes, which could be realized only by adjusting the ratios of the reagent concentration.[23] In addition to the rational chemical confined growth along some specific directions, with the help of orientation attachment and Ostwald ripening, some new nanostructures can be generated. Gao developed such a way to grow well-defined cubic hematite single crystals via oriented aggregation of nanorods by sharing common {012} faces.[24]

In this paper, with the use of simple organic alcohol solvent, we present some new approaches to rationally control the growth of hematite single crystals exhibiting a systemic shape evolution and consequently optical properties modification. The adsorption ability of species on (0001) planes is suggested to be selectively modified, and thus the nanocrystal shape can be tuned from nanoplates to nanograins with a continuing appearance probability of (0001) surface areas. In addition, a shape change can also be successfully achieved by ripening in a suitable solvent.

II. Experimental Section

Synthesis. Iron trichloride ($FeCl_3 \cdot 6H_2O$ Guangdong Guanghua Chemical Co.), ethanol (Tianjin Fuyu Chemical Co.), and sodium acetate (CH_3COONa, Guangdong Guanghua Chemical Co.) all A.R. grade were used as starting materials without further purification. In a typical synthesis of α-Fe_2O_3 hexagonal nanoplates, 0.273 g of $FeCl_3 \cdot 6H_2O$ (1.0 mmol) was dissolved under vigorously magnetic stirring in ethanol (10.0 mL) with a trace addition of water (0.7 mL). Until completely dissolved, 0.8 g of sodium acetate was added while stirring. The mixture was sealed in a Teflon-lined stainless steel autoclave (25 mL) and maintained at 180 °C for 12 h for solvothermal crystallization. Following natural cooling to ambient temperature, the resulting solid products were washed with distilled water and ethanol several times, respectively, and finally dried in a desiccator at 60 °C for ca. 10 h for characterization.

Characterization. The products were characterized by powder X-ray diffraction (XRD), scanning electron microscopy (SEM), transmission electron microscopy (TEM), and high-resolution TEM (HRTEM). XRD patterns were recorded with a Rigaku D/MAX 2200 VPC diffractometer using Cu Kα radiation (λ = 0.15045 nm) and a graphite monochromator. SEM images were taken with a FEI Quanta 400 Thermal FE environmental scanning electron microscope. Samples were gold-coated prior to the SEM analysis. TEM images were prepared on a JEM-2010HR transmission electron microscope operated at an accelerating voltage of 200 kV. The microscope is equipped with Oxford EDS spectrometer and Gatan GIF Tridiem systems for both structural and chemical analysis. TEM samples were prepared by dispersing the powders on holey carbon film supported on copper grids.

The infrared optical properties were measured on EQUINOX 55 IR spectrometer using KBr pellet technique. Raman spectroscopy was measured in the backscattering geometry utilizing a Leica microscopy system equipped with a 50× objective in Renishaw inVia spectrometer. The wavelength of the irradiating argon ion laser was 514.5 nm, and the spectra resolution was 1 cm^{-1}.

(11) Zheng, Z.; Chen, Y. Z.; Shen, Z. X.; Ma, J.; Sow, C. H.; Huang, W.; Yu, T. *Appl. Phys. A-Mater.* **2007**, *89*, 115–119.
(12) Wang, J.; White, W. B.; Adair, J. H. *J. Am. Ceram. Soc.* **2005**, *88*, 3449–3454.
(13) Tang, B.; Wang, G. L.; Zhuo, L. H.; Ge, J. C.; Cui, L. J. *Inorg. Chem.* **2006**, *45*, 5196–5200.
(14) Lu, L.; Li, L. P.; Wang, X. J.; Li, G. S. *J. Phys. Chem. B* **2005**, *109*, 17151–17156.
(15) (a) Mitra, S.; Das, S.; Mandal, K.; Chaudhuri, S. *Nanotechnology* **2007**, *18*, 1–9. (b) Vayssieres, L.; Beermann, N.; Lindquist, S. E.; Hagfeldt, A. *Chem. Mater.* **2001**, *13*, 233–235. (c) Fan, H. M.; You, G. J.; Li, Y.; Zheng, Z.; Tan, H. R.; Shen, Z. X.; Tang, S. H.; Feng, Y. P. *J. Phys. Chem. C* **2009**, *113*, 9928–9935. (d) Yin, W. Y.; Chen, X.; Cao, M. H.; Hu, C. W.; Wei, B. Q. *J. Phys. Chem. C* **2009**, *113*, 15897–15903. (e) Cao, M. H.; Liu, T. F.; Gao, S.; Sun, G. B.; Wu, X. L.; Hu, C. W.; Wang, Z. L. *Angew. Chem., Int. Ed.* **2005**, *44*, 4197–4201.
(16) (a) Zhou, H. J.; Wong, S. S. *ACS Nano* **2008**, *2*, 944–958. (b) Lee, S. M.; Cho, S. N.; Cheon, J. *Adv. Mater.* **2003**, *15*, 441–444. (c) Meng, L. R.; Chen, W. M.; Chen, C. P.; Zhou, H. P.; Peng, Q; Li, Y. D. *Cryst. Growth Des.* **2010**, *10*, 479–482.
(17) Jia, B. P.; Gao, L.; Sun, J. *J. Am. Ceram. Soc.* **2007**, *90*, 1315–1318.
(18) Hu, X. L.; Yu, J. C. *Adv. Funct. Mater.* **2008**, *18*, 880–887.
(19) (a) Jia, C. J.; Sun, L. D.; Yan, Z. G.; You, L. P.; Luo, F.; Han, X. D.; Pang, Y. C.; Zhang, Z.; Yan, C. H. *Angew. Chem., Int. Ed.* **2005**, *44*, 4328–4333. (b) Jia, C. J.; Sun, L. D.; Luo, F.; Han, X. D.; Heyderman, L. J.; Yan, Z. G.; Yan, C. H.; Zheng, K.; Zhang, Z; Takano, M.; Hayashi, N.; Eltschka, M.; Klaui, M.; Rudiger, U.; Kasama, T.; Cervera-Gontard, L.; Dunin-Borkowski, R. E.; Tzvetkov, G.; Raabe, J. *J. Am. Chem. Soc.* **2008**, *130*, 16968–16977.
(20) Sugimoto, T.; Wang, Y. *J. Colloid Interface Sci.* **1998**, *207*, 137–149.
(21) Wang, G. X.; Gou, X. L.; Horvat, J.; Park, J. *J. Phys. Chem. C* **2008**, *112*, 15220–15225.
(22) Wang, W.; Howe, J. Y.; Gu, B. H. *J. Phys. Chem. C* **2008**, *112*, 9203–9208.
(23) Wang, L. L.; Gao, L. *J. Phys. Chem. C* **2009**, *113*, 15914–15920.
(24) Jia, B. P.; Gao, L. *Cryst. Growth Des.* **2008**, *8*, 1372–1376.

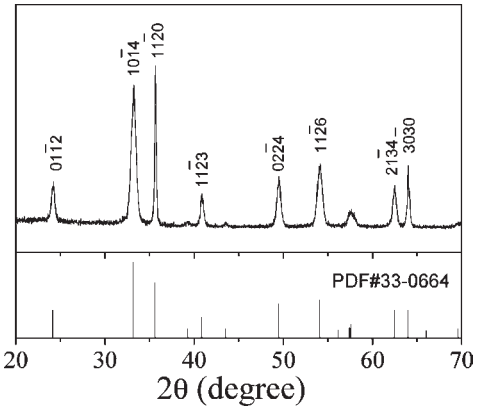

Figure 1. Powder X-ray diffraction (XRD) pattern of the product obtained through the typical growth procedure. The bars are from JCPDS Card No. 33-0664 for rhombohedral α-Fe_2O_3.

The laser light was focused to a spot size of ca. 1 μm diameter on the sample surface and the power was less than 2 mW. UV−vis−NIR diffuse reflectance spectra were obtained from Varian Cary-5000 spectrophotometer.

III. Results and Discussion

Structural Characterization of Nanoplates. The powder X-ray diffraction pattern (pXRD) in Figure 1 matches well with JCPDS card No. 33-0664 for rhombohedral α-Fe_2O_3 with $a = b = 0.5036$ nm and $c = 1.3749$ nm, confirming that the product is hematite without the presence of any impurities. The extended width of 10$\bar{1}$4 and 02$\bar{2}$4 diffraction peaks and the sharpness of *hki*0 [$\bar{i} = h + k$] ones implies a possibly preferred orientation along the *ab*-planes, which will be well characterized by electron microscopy (Figure 2).

From the SEM image in Figure 2a, we can see that the product consists of hexagonal nanoplates with a narrow size distribution. The dispersed particles in the TEM images (Figure 2b−f) are well crystallized in hexagonal plates with a width of around 200 nm and a thickness of around 10 nm. The aspect ratio is about 0.05, significantly small. Interestingly, the edges of a plate are not flat but wedge-shaped according to the images in the inset of Figure 2a when they are standing vertically. To address their growth behavior, the structures along two perpendicular directions, that is, the *c*-direction and *ab*-plane, were characterized by high-resolution TEM (HRTEM) and related fast Fourier transformation (FFT) (Figure 2b−f). Regular and thin hexagonal nanoplates can be observed from the TEM image in which they are lying horizontally (Figure 2b). The nanoplates are found to be single crystalline, suggested by the high-resolution TEM images and related FFT patterns in Figure 2c,e,f. The distinguishable lattice spacing of 0.25 nm in the HRTEM image in Figure 2c corresponds to {11$\bar{2}$0} planes, which is from the white square in Figure 2b for the well-developed hexagonal nanoplate. The FFT pattern in the inset at the left-bottom corner demonstrates six equivalent 11$\bar{2}$0 spots, suggesting that the basal up and down surfaces of the horizontally lying nanocrystal are ascribed to (0001) and (000$\bar{1}$) planes, respectively. On the first impression, the six surrounding edges of the nanoplate are smooth and they could be attributed to {11$\bar{2}$0}. However, when the nanoplates are vertically located (Figures 1a and 2d),

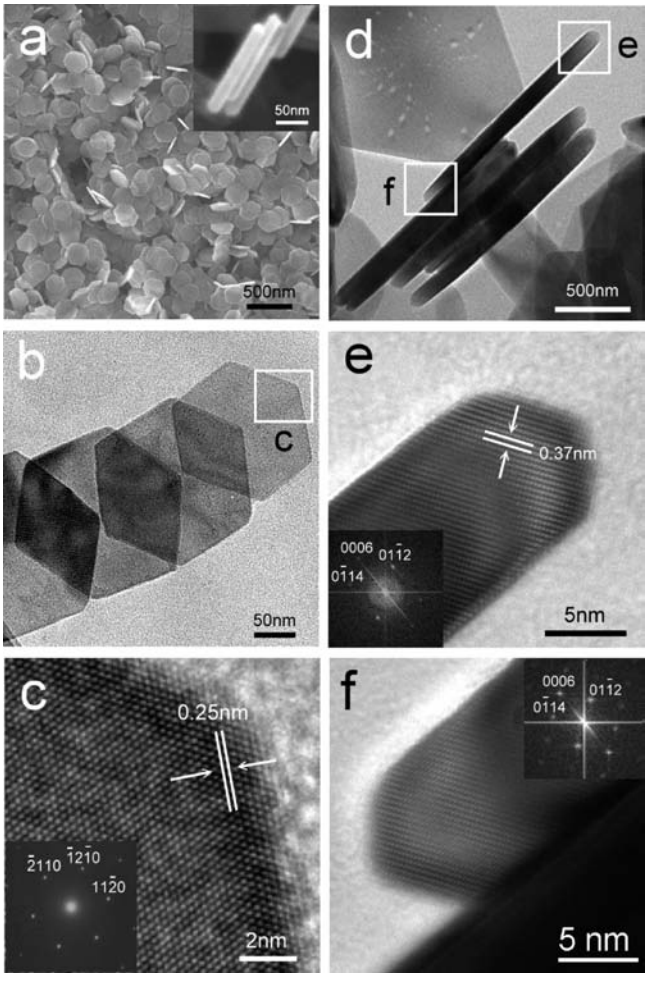

Figure 2. (a) SEM image of uniform nanoplates with an inset showing the free-standing side surfaces. (b) TEM image of several horizontally lying nanoplates and (c) HRTEM image and its related FFT pattern from the white square along the [0001] zone axis. (d) TEM image of several vertically standing nanoplates. (e, f) HRTEM images and their related FFT patterns from the opposite white squares in (d) along the [2$\bar{1}\bar{1}$0] zone axis.

the wedge-shaped projection of outer edges are observed, implying the side surfaces are enclosed by neither six {10$\bar{1}$0} nor {11$\bar{2}$0} facets but others. The HRTEM images in Figure 2e,f are taken from both edges (denoted by white squares) of a nanoplate in Figure 2d. The FFT patterns confirm the single-crystalline nature and the nanoplate is standing on [10$\bar{1}$0] via a side view. The up-edge in Figure 2e and the down-edge in Figure 2f are very smooth. The clear lattice fringes of 0.37 nm along the crystal surface on either edge definitely corresponds to {10$\bar{1}$2} planes in the HRTEM (Figure 2e,f) from either of two opposite side parts denoted by white squares in Figure 2d. The outmost surface enclosed by the {10$\bar{1}$2} plane is quite smooth, suggesting the exposed outside surfaces can be attributed to {10$\bar{1}$2} lattice planes for each nanoplate. However, the outlines of other down and up outside surfaces (Figure 2, panels e and f, respectively) are not flat and the tips of the wedge shape are not sharp, and thus the other six outside surfaces cannot be definitely indexed.

Because of less bonding of outside surface atoms on such a thin nanoplate, these atoms at the edges of each

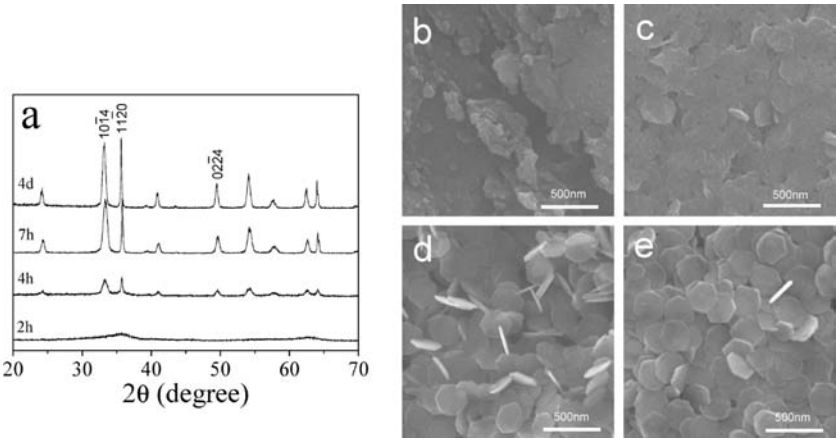

Figure 3. Powder XRD patterns (a) and SEM images (b−e) of the products from different periods of reactions for time-dependent investigation: (b) 2.0 h, (c) 4.0 h, (d) 7.0 h, and (e) 4.0 days.

$\{10\bar{1}2\}$ plane are quite active and try to find some new equilibrium positions to balance the forces. It can be found that the down outside surface in Figure 2e and the up outside surface in Figure 2f are both not smooth. Detailed investigation from magnified HRTEM images (Supporting Information, Figure S1) reveals a terrace−ledge−kink (TLK) surface structure at either such edge. The terraces are considered to be on the $\{10\bar{1}2\}$ planes and the ledges to be on $\{10\bar{1}4\}$ planes. Thus, it is reasonable to briefly define each nanoplate to be enclosed by larger ± (0001), smaller $\{10\bar{1}2\}$, and possible $\{10\bar{1}4\}$ planes. Hematite nanocrystals bound by $\{10\bar{1}2\}$ have been well described previously. These crystals were generally crystallized in cubic or rhombic shapes, and they were considered to appear with $[10\bar{1}4]$ diagonal growth direction.[23,24]

Growth Mechanism. Time-Dependent Growth. In order to understand the growth mechanism, several time-dependent experiments were performed (Figure 3). If the reaction was carried out for only 2 h, there are two bands around 36 and 63°/2θ in the XRD pattern of the product (Figure 3a, 2h). This suggests an amorphous product was formed. There are irregular and fine particles in the product as illustrated in Figure 3b. Actually, these fine particles aggregated, and some thin platelike species could be detected (Supporting Information, Figure S2). If the reaction was extended to 4 h, the powder XRD pattern shows that the hematite phase appears (Figure 3a, 4h). The hematite particles with hexagonal plate embryos emerged from these fine amorphous particles (Figure 3c). Inside a hexagonal plate, the particles self-assembled with a perfect orientation attach ment behavior, which was proved by evidence of a single-crystal-like selected area electron diffraction (SAED) pattern and HRTEM image with FFT pattern (Supporting Information, Figures S2 and S3). After continuing the reaction to 7 h, more perfect hexagonal plates with a clear framework were obtained (Figure 3d) and the powder XRD pattern still exhibits sharp $hki0$ $[\bar{i} = h + k]$ diffraction and diffused $10\bar{1}4$ and $02\bar{2}4$ diffraction peaks (Figure 3a, 7h). With further aging, real single crystalline hexagonal nanoplates were obtained (Figure 2). This hexagonal platelike nanostructure is quite stable, and it can be preserved under the autoclaving aging for a long time. Herein, after 4 days' aging, the outer edges of the hexagonal plates tend to be clearer and the larger up/down surfaces completely remain (Figure 3e). The evidence of the nearly unchanged feature of the XRD pattern in Figure 3a, 4d as compared to that in Figure 3a, 7h further suggests the high stability of the platelike nanostructure in the solvothermal condition.

The Addition of Water. The presence of trace water plays a significant role in facilitating the nucleation and growth of hematite nanoplates. Figure 4 shows the powder XRD patterns and SEM images of the products obtained for time-dependent investigation without the presence of water. Without the presence of any water in the ethanol solvent, phase-pure hematite cannot be obtained under the identical growth conditions as described in the above section (Figure 3). The growth of hematite in pure organic ethanol is considerably delayed (Figure 4). After even half a day's reaction, the product was mainly an amorphous phase (Figure 4a, 12h). The particles in the product appeared as spheres with a diameter of ca. 2.0 μm (Figure 4b). After one day, a hematite phase appeared (Figure 4a, 1d) and plate-like embryos emerged on the spherical particle surfaces (Figure 4c). After 3 days, hematite existed as the major phase with a trace of amorphous mixture. The free-standing nanoplates on the spherical amorphous precursor should be attributed to hematite. Pure hematite phase could be identified after an extremely long solvothermal growth of up to 6 days (Figure 4a, 6d and 4e). The slow growth behavior affords us a feasible chance to investigate detailed evolution of the hematite nanoplates. Instead of nanoplates in Figure 3, microspheres composed of mainly amorphous products were isolated after 12 h (Figure 4a). In previous literature, α-Fe_2O_3 was usually considered to be converted from oxyhydroxide via wet chemistry.[13,25] A direct transformation of amorphous iron precursors to crystalline hematite was rarely reported.[22] To detect the intermediate amorphous microspheres, Raman spectroscopy was employed. There are several polymorphs of Fe(III) oxide or oxyhydroxide (e.g., γ, ε, β, α-Fe_2O_3, α-FeOOH, γ-FeOOH and so on), which exhibits distinctive Raman soft modes. Therefore, it is possible to distinguish them by Raman study even though they are identified to be amorphous by X-ray

(25) (a) Li, Z. M.; Lai, X. Y.; Wang, H.; Mao, D.; Xing, C. J.; Wang, D. *Nanotechnology* **2009**, *20*, 1–9. (b) Chen, D. H.; Chen, D. R.; Jiao, X. L.; Zhao, Y. T. *J. Mater. Chem.* **2003**, *13*, 2266–2270.

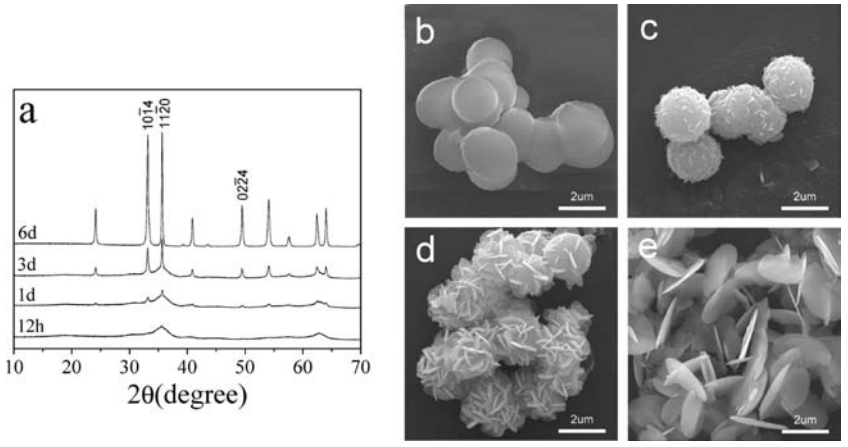

Figure 4. Powder XRD patterns (a) and SEM images of the products from pure solvothermal growth for different periods: (b) 12 h, (c) 1.0 d, (d) 3.0 d, and (e) 6.0 d.

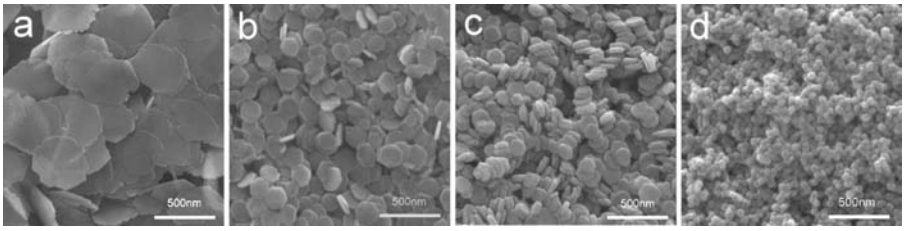

Figure 5. SEM images of hematite products grown from the solvent of ethanol with an addition of (a) 0.3 mL, (b) 0.7 mL, (c) 1.2 mL, and (d) 2.5 mL of distilled water. The volume of ethanol is kept at 10.0 mL and the use of sodium acetate is 0.8 g.

diffraction facility. For the microspherical sample, the Raman peaks at 220, 287, 393, 498, 603, and 1304 cm^{-1} (Supporting Information, Figure S4) all correspond to α-Fe_2O_3.[26] Details will be described below. The presence of other phases failed to be detected for the amorphous sample.

With the solvothemal growth continuing, the XRD diffraction peaks attributed to hematite tend to be stronger and sharper, and more and more free-standing nanoplates appear from the surface of each amorphous microsphere (Figure 4b−d). At the early growth stage of hematite, quite a number of nanoplates vertically grew from the surface of each microsphere (Figure 4b) and with further growth, well-developed nanoplates were situated in a cross way with each other to form a pinecone-like sphere. Thus, we are sure that there is a reversed growth progress during the crystallization of the aimed hematite nanoplates. A similar phenomenon was observed during the reversed crystal growth of zeolite analcime and zeolite A.[27] As previously, an aggregation of solid material was followed by surface crystallization and crystallization extension from surface to core.[27] The developing route is not to a single crystal or similar but to a sphere-like aggregate consisting of intersectant nanoplates on the surface. With a continuing growth of up to six days, more defined nanoplates are developed and most of them were separated from each other. However, these nanoplates look like thin circle pancakes but not hexagonal plates.

On the basis of the above discussion, we are convinced that the addition of water can surely promote the hydrolysis of $FeCl_3$ and the crystallization of hematite. Thus, the presence of water in the solvent has a great effect on the growth of hematite nanoplates. In addition to accelerating the transformation of amorphous precursory material to the hematite nanoplates, water molecules also significantly impact the growth behavior of hematite nanocrystals (Figure 5). The hematite crystal shapes have a sequential variation from nanoplates to nanograins with an increase of aspect ratios. With the addition of water in the volume from 0.3 to 2.5 mL into the solvent, the diameters of nanocrystals decrease from ca. 400 to 40 nm and the thickness increases from ca. 8 to 40 nm (Figures 5 and 6). The aspect ratio changes remarkably from ca. 0.02 to 1.0, in a magnitude of 50. The appearance of $\{10\bar{1}2\}$ surfaces becomes more significant while that of hexagonal {0001} ones become much smaller (Figure 6, bottom). Correspondingly, the $10\bar{1}4$ diffraction peaks tend to be narrower, while $hki0$ $[\bar{i} = h + k]$ ones tend to be wider with the addition of water (Supporting Information, Figure S5). The role of the presence of water is quite considerable in the growth of such polyhedral nanocrystals.

The above results indicate that the growth along either the 0001 or $000\bar{1}$ direction is considerably retarded for the anisotropic nanostructure, that is, nanoplates, in Figure 2. Generally speaking, the production of highly anisotropic nanoparticles has been achieved using growth inhibitors such as organic surfactant or templates,[1,5,28] because they can confine the growth along some specific directions. However, in the present work, neither template nor

(26) (a) Cvelbar, U.; Chen, Z. Q.; Sunkara, M. K.; Mozetic, M. *Small* **2008**, *4*, 1610–1614. (b) Spray, R. L.; Choi, K. S. *Chem. Mater.* **2009**, *21*, 3701–3709.

(27) (a) Chen, X.; Qiao, M.; Xie, S.; Fan, K.; Zhou, W.; He, H. *J. Am. Chem. Soc.* **2007**, *129*, 13305–13312. (b) Greer, H.; Wheatley, P. S.; Ashbrook, S. E.; Morris, R. E.; Zhou, W. Z. *J. Am. Chem. Soc.* **2009**, *131*, 17986–17992.

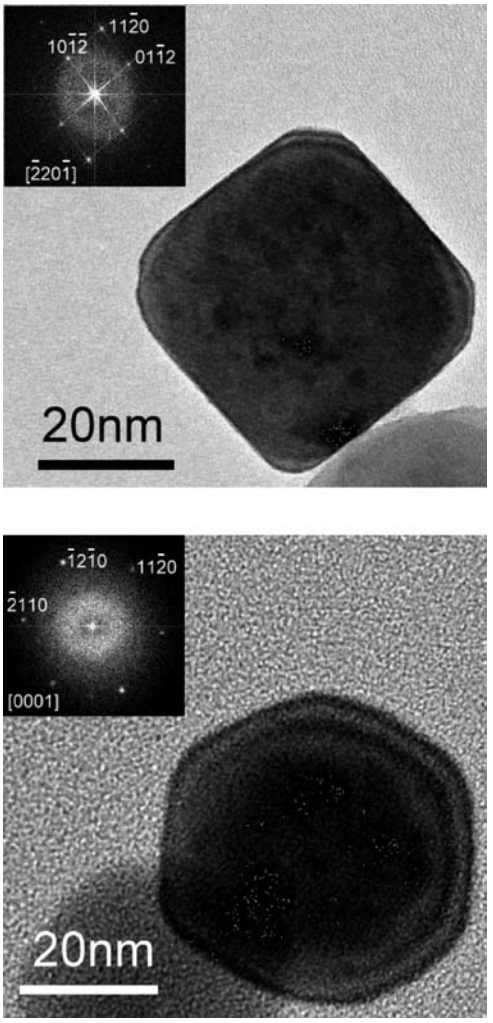

Figure 6. HRTEM images and related FFT patterns of a typical nanograin along $[\bar{2}20\bar{1}]$ (top) and [0001] (bottom) directions, respectively.

organic surfactant is used in all growth processes. The successful growth of nanoplates may be ascribed to the following reasons. First, the slow growth along the ⟨0001⟩ direction is inherently because of the low surface energy of (0001) surfaces. Second, it is proposed herein that the confined growth along the ⟨0001⟩ direction also results from the inherent polar crystallographic structure of α-Fe_2O_3 and the organic solvent. In α-Fe_2O_3, Fe^{3+} and O^{2-} ions are arranged alternatively along the *c* axis (Supporting Information, Figure S6). The larger up/down surfaces are terminated either by Fe^{3+} or O^{2-} ions, and there are net ionic charges on either surface. Consequently, either the (0001) or $(000\bar{1})$ surface of α-Fe_2O_3 is a polar plane.[18] If we suppose that (0001) planes are terminated by iron atoms and $(000\bar{1})$ by oxygen ones, we can speculate that alcohol molecules with oxygen atoms at the end, which have lone pair electrons, should have a nucleophilic affinity to surface iron atoms on (0001) planes. And subsequently, alcohol molecules confine the growth along ⟨0001⟩ directions and large ± (0001) facets appear. However, the fully terminated $(10\bar{1}2)$ surfaces are covered by mono- or three-coordinated oxygen atoms

(28) Gong, J. Y.; Guo, S. R.; Qian, H. S.; Xu, W. H.; Yu, S. H. *J. Mater. Chem.* **2009**, *19*, 1037–1042.

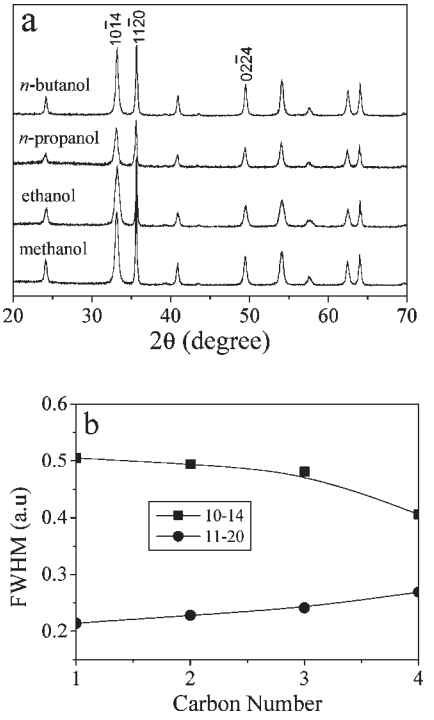

Figure 7. (a) Powder XRD patterns of the products grown from the solvent of different alcohols. (b) The variation of the full width at half-maximum (fwhm) of $10\bar{1}4$ and $11\bar{2}0$ diffractions with an increase of carbon number on the alkyl chain in alcohol molecules.

with which the oxygen atom in each ethanol molecule has an electrostatic repulsion (Supporting Information, Figure S7). Thus, the vertical growth along the *c*-axis is confined, but the radial one along the *ab*-plane is enhanced. And consequently, the growth of the nanoplate is achieved. However, with the addition of water into the reaction system, each water molecule plays an intermediate connection to bridge one terminating oxygen atom on a $(10\bar{1}2)$ surface and an ethanol molecule through hydrogen bonding. Correspondingly, with the addition of water, the radial growth along *ab*-planes is retarded and more $(10\bar{1}2)$-terminated facets appear (Figures 5 and 6).

Alcohol Solvents on the Growth. As stated above that the presence of ethanol molecules can confine the growth vertically, we can speculate that the greater the polarity of alcohol molecules is, the larger the top-bottom surfaces are, the thinner the nanoplates are, and the smaller the aspect ratios are. It has been well established that the polarity of alcohol molecules decrease as the length of the alkyl chain decreases. Several controlled experiments were performed to test the possibility of alcohol molecules on the growth of nanoplates. In these trial experiments, ethanol was replaced by methanol, *n*-propanol, and *n*-butanol as solvent, respectively. The pXRD data (Figure 7a) show us that all the products are hematite α-Fe_2O_3, but the evidence of an increase of full width at half-maximum (fwhm) of $11\bar{2}0$ and decrease of that of $10\bar{1}4$ diffraction peaks is obtained (Figure 7b), implying a continuing decrease of width and increase of thickness. The results of SEM observation visibly indicate a monotonic decrease of the aspect ratios of nanocrystals with the change of solvent from methanol to *n*-butanol (Figure 8). The nanoplates grown in methanol present the largest basal surface area and smallest thickness, while those grown in

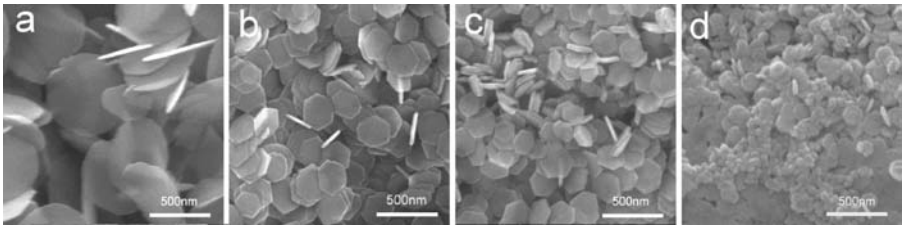

Figure 8. SEM images of the products grown from the solvent of (a) methanol, (b) ethanol, (c) *n*-propanol, and (d) *n*-butanol, respectively.

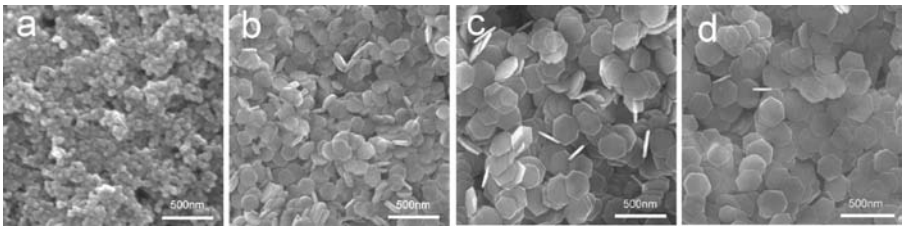

Figure 9. The addition of sodium acetate (a, 0.4 g; b, 0.8 g; c, 2.0 g; and d, 4.0 g) on the shapes of resultant α-Fe_2O_3 nanocrystals synthesized at the typical growth procedure with the addition of 1.0 mL of distilled water.

n-butanol present the smallest (0001) surface area and largest thickness. That is to say methanol molecules have the greatest affinity on the (0001) hematite plane and the greatest ability to confine the growth of hematite nanocrystals along the ⟨0001⟩ direction. The results coincide with our above rational speculation. However, if the alcohol was used with a much longer alkyl chain, such as *n*-butanol, the product was not uniform and some granular particles emerged.

Sodium Acetate on the Growth. It has been extensively established that carboxylic anions have a strong chelating ability to transition metal ions. The presence of acetate anions in the growth medium might have a strong ability to coordinate the surface ion atoms on (0001) planes and thus retard the growth of hematite nanocrystals along the ⟨0001⟩ directions. The IR spectra show us the vibration adsorption of the carboxylic anions on hematite surface, which will be further pointed out in the following section (section 3.4).

If retarded growth is achieved, the nanocrystals with a larger (0001) surface will tend to be obtained with an increasing amount of sodium acetate in the reaction mixtures. The results in Figure 9 unambiguously support the hypotheses, in which Fe^{3+} concentration, reaction temperature, and the amount of ethanol and water were kept constant as those in Figure 2 as described in Experimental Section for the typical growth while the quantity of sodium acetate changed from 0.4 to 4.0 g. That is, the amount of sodium acetate also has an important effect on the hematite nanostructures (Figure 9). If the amount of sodium acetate is 0.4 g, the product is small nanoparticles. With a further increase of the amount of sodium acetate from 0.8 to 2.0 g, the resultant nanocrystals are flaky and their diameter and thickness tend to be larger and smaller, respectively. This demonstrates that the addition of sodium acetate could confine the growth along the ⟨0001⟩ direction and promote that along the *ab*-plane. However, if the surfaces of the (0001) planes are completely covered by acetate ions, the further addition of the sodium acetate may play a negligible role to confine the growth of the two-dimensional nanoplates. For example, if the addition amount of sodium acetate is increased up to 4.0 g, the flaky shape of nanocrystals in the product does not have distinct modification (Figure 9d) as compared to that from the growth medium with 2.0 g of sodium acetate (Figure 9c).

The Aging in Distilled Water and Ethanol. To further address the effect of water and alcohol on the aging of these nanoplates, 0.5 mmol (0.08 g) of as-synthesized nanoplates (Figure 2) was added to 10 mL of distilled water and of ethanol (inside 25 mL Teflon cup), respectively. After aging at 180 °C for 7 days, the resultant nanocrystals appear with quite different final shapes. The edges of the nanoplates from water tend to be round, the nanoplates themselves tend to be thicker, and the diameters tend to be smaller (Figure 10a). It is possible that there is a mass transport from side surfaces to basal surfaces.[29] Previously, we proposed 1D/2D ripening of rutile TiO_2 nanorods during hydrothermal aging, in which the top/end parts of rutile nanorods gradually resolved and side-surface grew. The rutile nanorods became fatter but shorter, and the aspect ratio varied to be smaller and smaller during hydrothermal aging.[30] Herein, there is a 2D/1D ripening. That is, the side surfaces gradually dissolved and the mass was gradually transported to the basal top (or bottom) surfaces. Thus, we can imagine that each hematite nanocrystal grows along two opposite ⟨000$\bar{1}$⟩ directions from the same oxygen-terminated (000$\bar{1}$) plane, which serves as the symmetrical center (Figure 10b). However, even under higher saturation, the use of either alcohol molecules or carbonate ions, which can be adsorbed on the two opposite (0001) planes, can confine the growth along both ⟨0001⟩ directions. Thus, the growth parallel to the *ab*-plane is enhanced during the growth stage. During the aging stage under lower saturation in water, the side surface edges gradually redissolve and "a mass transport" takes place from the side surface to both top (0001) surfaces (Figure 10a and

(29) Peng, Z. A.; Peng, X. G. *J. Am. Chem. Soc.* **2001**, *123*, 1389–1395.
(30) Yang, X. F.; Konishi, H.; Xu, H. F.; Wu, M. M. *Eur. J. Inorg. Chem.* **2006**, 2229–2235.

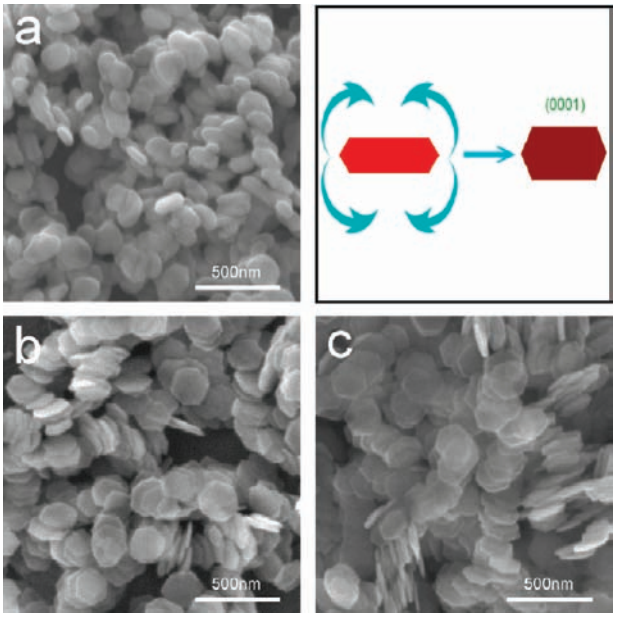

Figure 10. SEM images of the resultant samples after hydrothermal and ethanol-thermal aging of the typical product in Figure 2 at 180 °C for 7 days: (a) in water with a scheme showing 2D/1D ripening (right), (b) in ethanol, (c) in water but with the addition of sodium acetate.

scheme). However, the hexagonal flaky frameworks remain after ethanol-thermal aging or in water in the presence of CH_3COONa (0.02 mol·L^{-1}) even for one week (Figure 10b,c). This is because the growth along ⟨0001⟩ directions is still retarded in ethanol or CH_3COO^-. Conclusively, the nanostructures of hematite can be rationally finely controlled and modified based on fundamental crystallography and surface chemistry on either of two stages: growth or aging period.

Optical Performance. Fourier Transform Infrared (FTIR) Spectra. The above experimental results suggest that the growth of α-Fe_2O_3 can be modulated by the use of organic alcohol solvents and the presence of sodium acetate and distilled water. It has been well established the chemisorption of molecules and/or ions on crystal surface can modify the growth of a crystal plane due to surface energy. Fourier transform infrared (FTIR) spectra can detect the presence of these species on the surface and reveal the morphological evolutions due to the vibration mode along or perpendicular to one specific direction such as the *c*-axis. Four typical FTIR spectra of samples grown from the ethanol solvent with an increasing addition of distilled water (Figure 5) are shown in Figure 11 and Supporting Information, Figure S8. These absorptions in infrared ranges from 800 to 4000 cm^{-1} are ascribed to absorbed molecules on hematite nanocrystal surfaces. The wide bands around 3413 cm^{-1} are assigned to stretching vibrations of -OH, which primarily originates from the surface hydration and alcohol layers. The weak band in the range of 2800−3000 cm^{-1} is considered to come from C−H vibration.[31] The weak peaks at 1629 and 1420 cm^{-1}, corresponding to asymmetrical and symmetrical vibration of carboxylate groups, implies a chemical

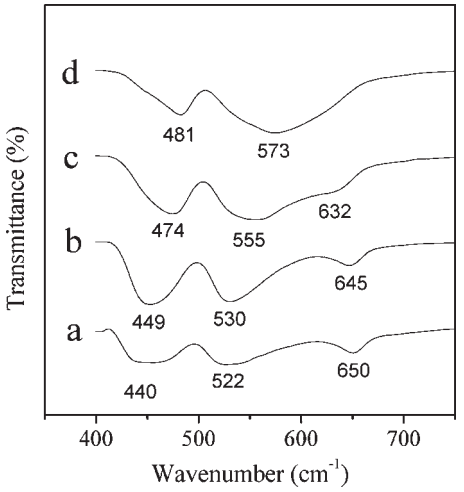

Figure 11. FTIR spectra of the hematite products grown from the solvent of ethanol with an addition of (a) 0.3 mL, (b) 0.7 mL, (c) 1.2 mL, and (d) 2.5 mL of distilled water as shown in Figure 5.

coordination of oxygen atom in acetate anions to iron atoms in unidentate mode.[23]

The strong and broad absorptions in the range of 400−800 cm^{-1} are from the inherent lattice vibrations of α-Fe_2O_3. Group theoretical analysis predicts that there are six infrared active modes for α-Fe_2O_3 lattice vibrations, two polarized along the *c*-axis (∥ modes) and the four perpendicular to the *c*-axis (⊥ modes). The intensities of ⊥ mode are much stronger than those of the ∥ mode.[32,33] It has been well documented that the infrared optical properties of hematite are size- and shape-dependent, due to the polarization change induced by external electromagnetic field at crystal surface.[14,18,32,33] The as-prepared uniform α-Fe_2O_3 nanoplates and nanograins having a continuing shape evolution with decreasing (0001) surface areas and increasing aspect ratios offer a good opportunity to systematically observe the fine change of IR spectra (Figure 11). For the flaky sample grown with 0.3 mL of water, there are three bands at around 440, 522, and 650 cm^{-1}. The absorptions at 440 and 522 cm^{-1} are ⊥ mode while that at 650 is ∥ mode. This FTIR curve is quite similar to that from microsized platelet crystals in the early classical work by Wang and his co-workers.[33] In their work, the ∥ mode bands were much weaker than those ⊥ ones. The absorption peaks at 650 cm^{-1} disappeared when the particles crystallized in pseudocubes. Herein, the ∥ mode tends to be weaker and gradually disappears with the aspect ratio being larger. The strong absorption of ∥ mode at 650 cm^{-1} in our present work confirms the remarkable flaky nanostructure. Both of the two absorption bands of ⊥ modes shift systematically to lower frequencies from nanoplates to nanograins with the increasing *c*/*a* aspect ratios as the increasing addition of distilled water in the growth system from 0.3 to 2.5 mL (Figure 5). In contrast, the ∥ mode has a tendency to higher frequencies. In addition, its intensity tends to be weaker and its absorption disappears while 2.5 mL of distilled water is present. With respective shifts to higher

(31) Liang, X.; Wang, X.; Zhuang, J.; Chen, Y. T.; Wang, D. S.; Li, Y. D. *Adv. Funct. Mater.* **2006**, *16*, 1805–1813.

(32) Hayashi, S.; Kanamori, H. *J. Phys. C: Solid State Phys.* **1980**, 1529–1538.

(33) Wang, Y.; Muramatsu, A.; Sugimoto, T. *Colloids Surfaces A* **1998**, *134*, 281–297.

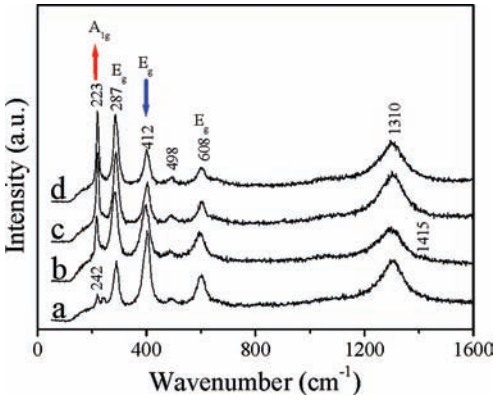

Figure 12. Raman spectra of the hematite products grown from the solvent of ethanol with an addition of (a) 0.3 mL, (b) 0.7 mL, (c) 1.2 mL, and (d) 2.5 mL of distilled water as shown in Figure 5.

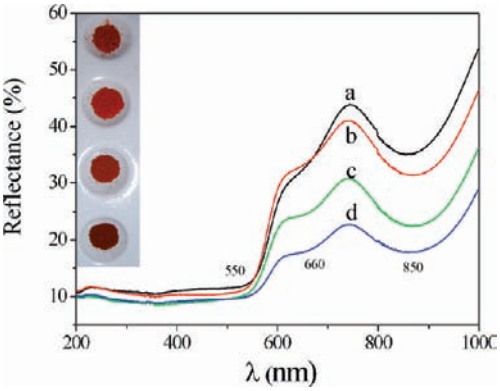

Figure 13. Diffuse reflectance spectra of hematite nanocrystals with a systemic shape change from nanoplate (a) to nanograin (d) through modifying the growth condition with adding (a) 0.3, (b) 0.7, (c) 1.2, and (d) 2.5 mL of distilled water (see Figure 5).

and lower frequencies, the two absorption bands initially at 522 and 650 cm^{-1} (Figure 11a) consequently merge together into one wide band around at 573 cm^{-1} (Figure 11d). Thus, there are two strong absorptions at 481 and 573 cm^{-1} with ⊥ modes in the FTIR spectrum of the nanograin sample (Figure 5), which is quite similar to those of pseudocubes in Yu's work[18] and Wang's works.[33] The strong influence of shape on IR absorptions in our present work with a shape change from nanoplate to nanograin, that is, the ⊥ peaks shift to a higher frequency, while ∥ peaks shift to a lower frequency, is identical to the previous theoretical calculation and experimental results.[32,33] Therefore, the FTIR feature can be tuned with the control of shapes and aspect ratios, and inversely the nanostructures may be predicted with the help of FTIR spectra even without straightforward observation under a microscope.

Raman Spectra. As the FTIR vibration is highly shape-dependent, it can be expected that Raman spectra deduced from vibration are also shape-dependent. However, systematic investigation of shape-change on Raman spectra has been rarely reported. The α-Fe_2O_3 crystallized as a corundum-typed structure (*R*3-C) is the most common iron oxide on earth. The Raman spectra of α-Fe_2O_3 crystals have been extensively investigated, in which there are seven Raman-active vibration modes, two A_{1g} modes and five E_g ones. As predicated by group theory, the Raman bands at 223 and 498 cm^{-1} in our present work belong to two A_{1g} modes, while those at 242, 287, 412, and 608 cm^{-1} to E_g modes.[34] In Figure 12, relative intensity of the A_{1g} mode at 223 cm^{-1} increases sharply as compared with other Raman-active E_g modes, while more distilled water was added into the reaction feedstock. It is quite possible that the enhanced Raman absorption is attributed to the shape modifications. With a shape change from nanoplate to nanograin, the A_{1g} mode at 223 cm^{-1} is significantly enhanced. That is, the Raman vibrations with A_{1g} modes are highly reduced in the nanograins. It was reported in early works that the E_g mode at about 614 cm^{-1} significantly decreased as particle size decreased,[12] and both E_g and A_{1g} modes were greatly orientation-dependent.[34,35] In the *zz* configuration, only A_{1g} modes were allowed in a single crystal, while in the crossed *xz* and *yz* polarization, only the E_g modes were allowed and only a small residue of the intense 223 cm^{-1} A_g mode was observed.[35] In the present Raman spectrum of thinnest nanoplates, the intensity of 223 cm^{-1} A_g mode is remarkably weak, indicating the very small crystal thickness confines the A_{1g} vibration mode along the [0001] direction. Further detailed research on the relationship between Raman spectra and nanostructures is in progress. The LO line located at 655 cm^{-1} is Raman forbidden, and only the 2LO line can be observed. Because of resonance enhancement, the 2LO line, the broad band at around 1310 cm^{-1} appears apparently.[36] A weak shoulder band at 1415 cm^{-1} may be attributed to vibration of carboxylate groups. More examples are illustrated in Supporting Information, Figure S9.

Diffuse Reflectance Spectra (DRS). As described above, the vibration spectra, either FTIR or Raman one, are highly shape-dependent. It can be expected that the electronic spectra of hematite nanoparticles are also shape-dependent. It has been well established that the apparent color of hematite particles is significantly related to size and shape.[12] However, a systemic observation of sequent apparent color change has not been performed to the best of our knowledge. After increasing the addition of distilled water into the reaction system, the body color of as-grown powders tends to be dark. There is a color change from bloody brown to dark brown. The color changes like a concentration of blood, from dilute to concentrated liquid blood. This can be easily understood according to the diffuse reflectance spectra as shown Figure 13. The decrease of reflectance from curve *a* to curve *d* indicates that nanoplates have a higher ability to reflect light than do nanograins; that is, the nanograins have a higher ability to absorb visible light. This evidence suggests that (0001) surface planes may possess higher reflectance ability than other surface planes.

DRS can be employed to detect band gap. Below 550 nm, the reflectance is very low, and a sharp increase around 560 nm is observed. The sharp increase at around 560 nm tells us the band gap is around 2.2 eV. The slope with a slight shift to a longer wavelength tends to be slow

(34) Beattle, I. R.; Gilson, T. R. *J. Chem. Soc. A* **1970**, *A*, 980–986.
(35) Bersani, D.; Lottici, P. P.; Tosini, L.; Montenero, A. *J. Raman Spectrosc.* **1999**, *30*, 1043–1047.
(36) (a) McCarty, K. F. *Solid State Commun.* **1988**, *68*, 799–802. (b) Martin, T. P.; Merlin, R.; Huffman, D. R.; Cardona, M. *Solid State Commun.* **1977**, *22*, 565–567.

from spectrum a to d, representative of a detectable shape effect on the band gap. The wide absorption band around 660 nm (ca. 15152 cm^{-1}) in the red range is believed to arise from spin-forbidden ligand field transition, mostly likely $^6A_1$-$^4T_2$. The near-infrared range around 850 nm (ca. 11765 cm^{-1}) corresponds to another ligand field transition of Fe^{3+}, that is, $^6A_1$-$^4T_1$. From Figure 13, it is quite obvious that the absorption intensities for these ligand field transitions are systematically shape-dependent.

IV. Conclusions

Hexagonal α-Fe_2O_3 nanoplates with central symmetry on $(000\bar{1})$ have been successfully grown via a simple ethanolthermal route in the presence of trace water and with the addition of acetate sodium. They are enclosed by two large symmetric (0001) planes as basal surfaces and $(10\bar{1}2)$ as side surfaces. The presence of water in the organic solvent can highly facilitate the nucleation and modify the growth of the aimed α-Fe_2O_3 nanocrystals. The use of water can promote the growth while that of sodium acetate can confine the growth along the *c*-direction. The confined growth along this specific direction was attributed to the adsorption of acetate anions on (0001) surfaces. Thus, the shape of these nanocrystals can be finely tuned. The shape control can also be realized by the alternative use of various alcoholic solvent, such as methanol, *n*-propanol, *n*-butanol due to their different alkyl chain lengths, dipole moment, and consequently the strength of adsorption on (0001) planes. The aging of as-grown α-Fe_2O_3 nanoplates in either water or ethanol indicate that there is a promoted resolution of side-surface and regrowth of basal (0001) surface in water. By the suitable use of alcoholic solvent, distilled water, and acetate sodium during solvothermal growth and/or during post aging of as-grown nanoplates, the shape and favored growth orientation can be rational controlled and modified. Because of the confined Raman vibration of A_{1g} mode along the *c*-direction, the intensity of the A_{1g} mode tends to be weaker and weaker with a shape change from nanograin to nanoplate. As previously reported results, the growth orientation related FTIR absorptions can be significantly observed: the ⊥ peaks shift to a lower frequency while ∥ peaks shift to a higher frequency with the increase of aspect ratio. Probably because of the high reflectance ability of (0001) lattice planes, a consequent color change of the powdery product with the increasing of the aspect ratio was detected. The highly shape-dependent vibration spectra and electronic spectra will provide us with an alternative simple but feasible way to probe the possible shape of nanosized crystals without the help of electron microscopy.

Acknowledgment. This work is financially supported from National Natural Science Foundation (NNSF) of China and the Government of Guangdong Province for NSF and industry program (Nos. U0734002, 50872158, 8251027501000010).

Supporting Information Available: Additional XRD patterns, Raman spectrum, enlarged HRTEM, and structural models. This material is available free of charge via the Internet at http://pubs.acs.org.